Environmental Science Nano

Zero-Wastewater Capacitive Deionization: Selective Removal of Heavy Metal Ions in Tap Water Assisted by Phosphate Ions

Journal:	*Environmental Science: Nano*
Manuscript ID	EN-ART-06-2019-000730.R1
Article Type:	Paper
Date Submitted by the Author:	25-Aug-2019
Complete List of Authors:	Huang, Xingkang; University of Wisconsin Milwaukee Guo, Xiaoru; University of Wisconsin Milwaukee Dong, Qianqian ; Tongji University College of Environmental Science and Engineering, ; University of Wisconsin Milwaukee, Liu, Lianjun; A O Smith Corp Tallon, Rebecca; A O Smith Corp Chen, Junhong; University of Wisconsin Milwaukee

COMMUNICATION

Zero-Wastewater Capacitive Deionization: Selective Removal of Heavy Metal Ions in Tap Water Assisted by Phosphate Ions†

Received 00th January 20xx,
Accepted 00th January 20xx

DOI: 10.1039/x0xx00000x

Xingkang Huang, *‡[a] Xiaoru Guo, ‡[a] Qianqian Dong,[a] Lianjun Liu,[b] Rebecca Tallon,[b] and Junhong Chen*[a]

Removing trace toxic heavy metals such as Pb^{2+} completely from drinking water is important for protecting human health. However, healthy ions such as Ca^{2+} and Mg^{2+} in reasonable concentrations are beneficial to human health and thus do not need to be removed. Here we report a zero-wastewater capacitive deionization (CDI) technology using a thiol-functionalized graphene oxide/activated carbon (GO/AC) composite material for the selective removal of heavy metal ions in tap water. The thiol groups have a strong affinity to heavy ions (such as Pb^{2+}), leading to very high Pb removal selectivity against Ca^{2+} and Mg^{2+}. More importantly, native phosphate ions were found to significantly modify the CDI process in tap water. The presence of phosphate ions leads to the formation of Pb particulates with free ions in the tap water. During charging the particulates are removed by electrosorption onto cathodes while the accumulated Pb particulates are released upon discharging, forming precipitates by reacting with concentrated phosphate ions from anodes. The precipitates can be subsequently collected using filters equipped in the pipeline, thereby leading to a zero-wastewater CDI.

Environmental significance

Capacitive deionization (CDI) features low energy consumption, low life-cycle cost, high efficiency, high recovery rate, leading to its promising application in metal ion removal, water softening, and desalination. Heavy metal ions are poisonous to human health, especially to young children and pregnant women, and thus should be removed from drinking water. In contrast, healthy ions such as Ca^{2+} and Mg^{2+} should not be removed when their concentrations are within the benign concentration range. In this work, a novel concept of zero-wastewater CDI has been demonstrated to selectively remove lead ions against Ca^{2+} and Mg^{2+} by taking advantage of native phosphate ions in tap water. Compared with the traditional CDI having ~25% of concentrated wastewater, the new CDI process produces no wastewater. Compared with reverse osmosis (RO) systems that remove all ions, there is no need to add back healthy ions following the RO process. Therefore, the new CDI process is more economic, energy-efficient, and resource-saving while delivering safe water with desired level of minerals.

Heavy metal ions in drinking water are harmful to human health and should be reduced to below their action levels, e.g., 15 parts per billion (ppb) for lead (Pb), as recommended by the U.S. Environmental Protection Agency (US EPA).[1] According to the World Health Organization (WHO), Mg^{2+} and Ca^{2+} must be partially removed in drinking water to reduce hardness when their concentrations are higher than 30 and 80 parts per million (ppm), respectively.[2] However, the minimum content for Mg^{2+} and Ca^{2+} in drinking water is 10 and 30 ppm, respectively, and because of their benefits to human health, as recommended by WHO,[2] these ions do not need to be removed completely. In contrast, heavy metals such as Pb^{2+} are poisonous, even at low concentrations. Pb interferes with neurodevelopment, particularly by reducing intelligence quotient (IQ),[3] and thus requires additional attention. Because many aging water pipes in the US contain lead, the lead content in tap water is occasionally found to be higher than 15 ppb, especially in the early morning. For example, the lead content from first-draw samples at taps from 50 homes in Milwaukee (Wisconsin, US) in 2017 was up 130 ppb.[4] Due to the high cost for cities to replace aging water pipes, the selective removal of heavy metals from tap water is more effective and economical.

The selective removal of lead has been investigated extensively using methods such as polyethylene glycol methacrylate gel beads,[5] ethylenediamine-modified attapulgite,[6] sol-gel-derived ion-imprinted silica-supported organic-inorganic hybrid sorbent,[7] ion-imprinted silica sorbent

[a] Department of Mechanical Engineering, University of Wisconsin-Milwaukee, 3200 North Cramer Street, Milwaukee, WI, 53211, USA. E-mail: xkhuang@uwm.edu; jhchen@uwm.edu.

[b] A.O. Smith Corporation, Corporate Technology Center, 12100 W Park Place , Milwaukee, WI, 53224, USA.

‡ These authors contributed equally.

†Electronic Supplementary Information (ESI) available: [details of any supplementary information available should be included here]. See DOI: 10.1039/x0xx00000x

functionalized with chelating N-donor atoms,[8] bulk liquid membranes containing crown ether and oleic acid as carrier,[9] magnetic 2-hydroxyethylammonium sulfonate immobilized on γ-Fe_2O_3 nanoparticles,[10] natural clayey,[11] hydrous manganese dioxide,[12] α-MoO_3 porous nanosheets array,[13] and hollow mesoporous silica loaded with molecularly imprinted polymer.[14] However, only a few reports use the capacitive deionization (CDI) technology.[15-18]

Compared with other water-purifying techniques (e.g., reverse osmosis, RO), the advantages of CDI include a low lifecycle cost, the ability to remove a wide range of ionic contaminants, a high recovery rate, and low energy consumption. We have demonstrated the selective removal of lead ions in synthetic water (ultrapure water with target ion salts) using activated carbon with CDI in the presence of anion-exchange membranes (AEM-CDI).[16] In this study we explored the selective removal of lead ions in tap water with a single-pass mode. Compared with synthetic water, tap water is more complicated but close to practical applications. Our findings reveal that phosphate ions in tap water significantly affect the ability to remove lead ions. Upon charging, lead ions accumulate on cathodes and are then released at high concentrations during discharge and form precipitates with the concentrated phosphate ions from anodes. Unlike a conventional CDI, which typically requires discharging the concentrated solution as wastewater, the resulting phosphate precipitates can be easily collected with filters without discharging wastewater

Activated carbon (AC) electrodes exhibit selective removal of Pb^{2+} against Ca^{2+} and Mg^{2+}, but shows low selectivity.[16] Surface modification helps to improve the selectivity, but the large AC particles make it unsuitable. The cross-linking agents could be adsorbed into the deep micropores in the large AC particles. In contrast, graphene oxide (GO), consisting of a few C layers in thickness, is much more easily subjected to surface modification. More importantly, the thin GO sheets offer easier Pb release upon discharging compared with AC discharging Pb from the deep micropores. One of the major problems for GO is the agglomeration during drying, which makes it difficult to coat the electrodes with a doctor blade. It is also difficult to grind the aggregated GO sheets smaller than 50 μm, at which uniform coats can be achieved using the doctor blade. As a result, forming a GO/AC composite is an optimum choice for fabricating an electrode for selective removal of lead ions. Graphene-based materials have shown great interests in water treatment using CDI techniques.[19-23] Due to the high cost of graphene, a GO/AC composite can significantly reduce costs because AC is much cheaper than GO.

Experimental details can be found in the Supporting Information. The AC consists of micro-sized particles (typically 1-6 μm) with a porous surface (less than 10 nm), as shown in Figures S1a-c. The GO was functionalized by thiol groups using 3-(Mercaptopropyl)trimethoxysilane (MPS). The MPS possesses silane groups that have been widely used to functionalize GO through the condensation reaction[24-27] while the thiol groups in the MPS can selectively capture lead ions due to the strong affinity between lead ions and thiol groups. Compared with the

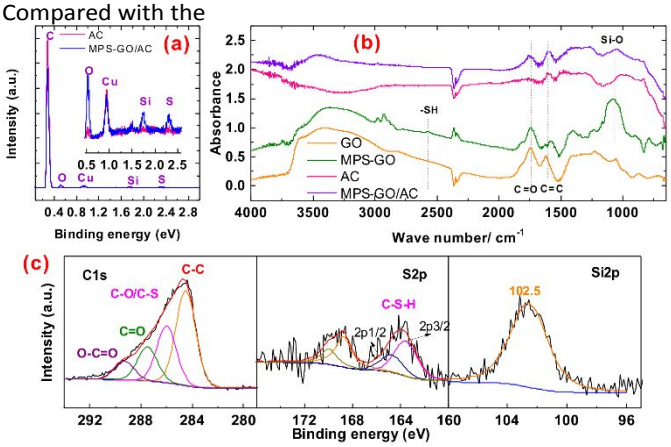

Figure 1. (a) EDS, (b) FTIR spectra of AC, GO, and MPS-GO/AC, and (c) XPS spectra of MPG-GO/AC.

AC, the MPS-GO/AC depicts similar morphology in low-magnification images; however, MPG-GO sheets were observed covering the surface of the AC (Figures S1d-f). Additional scanning electron microscopy (SEM) images of the MPG-GO/AC composite, shown in Figure S2, suggest incomplete coverage of the MPS-GO, but most of the AC was coated with the MPS-GO sheets.

The AC and the MPG-GO/AC were first examined by X-ray diffraction (XRD) and Raman spectroscopy, which did not show any information of the functional groups (Figure S3). Thus, energy dispersive X-ray spectroscopy (EDS) analysis was used to identify functional groups in the carbon materials. The C and O contents in the AC were 98.1 and 1.9 wt.%, respectively, suggesting relatively low O-containing groups (Figure 1c). In contrast, the C and O contents were determined to be 82.5 and 15.8 wt.%, respectively, confirming the increased O content in the MPS-GO/AC. In addition, Si and S were detected, with contents of 0.82 and 0.89 wt.%, respectively, due to the surface modification of the thiol groups from the MPS.

The evidence of the surface modification was also examined by Fourier-transform infrared spectra (FTIR). As shown in Figure 1d, the MPS-GO/AC composite presented a relatively strong C=O absorbance at 1,738 cm^{-1} compared with that of the AC; however, no obvious absorbance from -SH was observed, owing to the typical weak response of the -SH[28-32] and the low GO content (30 wt.%) in the MPS-GO/AC composite. Therefore, the FTIR of the GO and the MPS-GO were compared to find evidence of functionalized thiol groups. Two major peaks at 1,738 and 1,610 cm^{-1} in the FTIR of the GO were assigned to C=O and C=C,[33, 34] respectively; in contrast, a weak peak at 2,570 cm^{-1} in the MPS-GO resulted from the thiol group (-SH).[28, 30] In addition, the peak at 1,068 cm^{-1} was ascribed to Si-O,[35] indicating successful surface modification of the MPS on the GO surface. The successful surface graft of MPS was further confirmed by X-ray photoelectron spectroscopy (XPS). As shown in Figure 1e, the S 2p for C-S-H and the Si 2p for Si-O were observed at 164 and 102.5 eV,

respectively. Note that the peak for S 2p at approximately 169 eV is uncertain at this stage, but was reported to be originated from oxidized sulphur (-SOxH).[36] The CDI performance was tested using a lamellar cell, in which

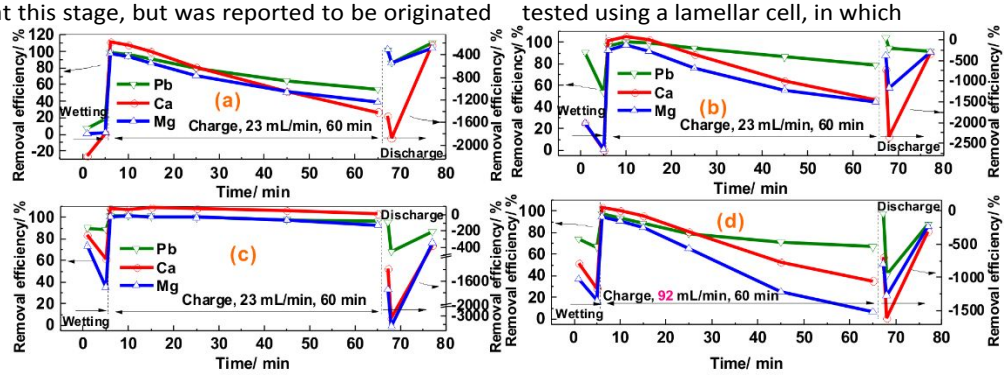

Figure 2. CDI performance with various electrodes: (a) Four-layer electrode cell with AC (b), Eight-layer electrode cell with AC (c), Four-layer electrode cell with functionalized graphene/AC composite, and (d) Four-layer electrode cell with functionalized graphene/AC composite at a high flow rate of 92 mL min^{-1}. The synthetic water was used by adding 1 ppm Pb^{2+}, 1 ppm Ca^{2+}, and 1 ppm Mg^{2+} in ultra-pure water. Only AEM was applied without cation exchange membrane (CEM). Note that the negative removal efficiencies during discharge indicate the ions were released from the electrodes because removal efficiency was defined by the concentration difference between the influent and the effluent, divided by the influent concentration (Equation S1). The related concentrations at the third point during discharge processes were the average concentrations of all the discharge water minus that was taken for the first two discharge samples; the discharge rate was thus calculated based on the ratio of total amount of each discharged ion to the total volume of collected solution (Equation S3).

multiple electrodes were stacked while the solution was pumped in from the bottom centre, spread to the four corners of the cell, and then finally flew out of the top centre. All the tests were conducted using the single-pass mode, because it is closer to the practical application compared with the batch mode.[37-39] The AC demonstrated selective Pb removal against Ca^{2+} and Mg^{2+}; however, the selectivity needs improvement [16]. Prior to demonstrating the CDI performance of the MPS-GO/AC composite in tap water, it was necessary to investigate its performance in synthetic water, namely pure water with Pb^{2+}, Ca^{2+}, and Mg^{2+}. As shown in Figure 2, applying four layers of AC electrodes achieved an average lead removal rate of 74.2 % with a discharge rate of 47% (Figure 2a). In contrast, applying four layers of MPS-GO/AC composite electrodes enabled the CDI cell to achieve an average lead removal rate of ~99% with a discharge rate of 34% (Figure 2c), which was even better than its performance with eight layers of AC electrodes (average Pb removal of 90%; Figure 2b).

The relatively lower discharge in the presence of the MPS-GO/AC is due to the strong affinity between the thiol and lead ions. Extended discharge time could provide a higher lead release (see below). Due to the nearly complete removal of all ions using the four-layer-electrode CDI cell with the MPS-GO/AC at 23 mL min^{-1}, no removal selectivity of Pb^{2+} against Ca^{2+} and Mg^{2+} can be observed (Figure S4). Therefore, a higher flow rate (92 mL min^{-1}) was introduced to the cell, resulting in significant removal selectivity of Pb^{2+} against Ca^{2+} and Mg^{2+}, plus an average lead removal rate of 78% with a discharge rate of 45% (Figure 2d). In other words, compared with the AC, the four-layer-electrode cell with the MPS-GO/AC showed a higher lead removal rate and improved Pb removal selectivity against Ca^{2+} and Mg^{2+} at quadruple the flow rate. This indicates the great benefit of the surface-modified GO. Note that the selectivity of Pb^{2+}/Mg^{2+} was much higher than that of Pb^{2+}/Ca^{2+} (Figure S4), which is related to the replacement mechanism for the selective removal of Pb^{2+}.[16] Ca^{2+} and Mg^{2+} possess a higher mobility than Pb^{2+}, thereby landing on the electrode sooner than Pb^{2+}; however, the Ca^{2+} and the Mg^{2+} arrived earlier at the electrode were replaced by the Pb^{2+} because it has a stronger affinity with the functional groups (such as thiol and carboxyl). Meanwhile, Mg^{2+} exhibited a water exchange rate five orders of magnitude slower than that for Ca^{2+} because of the stable inner hydration

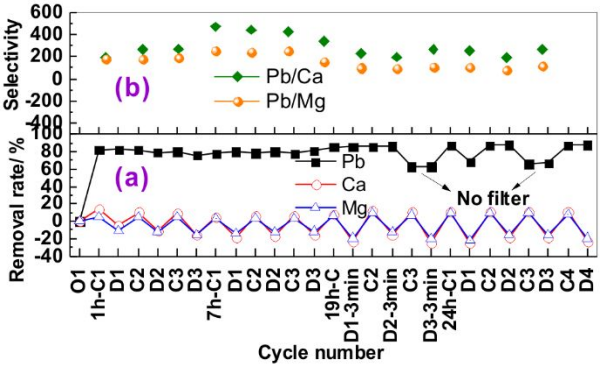

Figure 3. CDI performance of the MPS-GO/AC in tap water at a flow rate of 23 mL min^{-1}. (a) Removal rates during charge/discharge, in which C and D represents charge and discharge process, respectively, and (b) Pb removal selectivity against Ca^{2+} and Mg^{2+}. The sample solutions were taken at the 1st, 7th, 19th, and 24th hour with a typical charge time of 10 min and discharge time of 2 min. 3-min discharge time was applied at the 19th cycle. The solution was filtrated using filters to remove precipitates unless stated otherwise.

shell of Mg^{2+}.[16, 40, 41] As a result, Pb^{2+} could take more place of Mg^{2+} than that of Ca^{2+}, resulting in a higher Pb removal selectivity against Mg than Ca.

These encouraging results inspired us to further test the CDI performance of the MPS-GO/AC using tap water with regeneration processes, which is an approach toward practical applications. The water quality of the used tap water can be found in reports by Milwaukee Water Works.[42] The lead-contaminated tap water was simulated by adding 1 ppm of

Pb^{2+} into tap water from our office building, in which the Ca^{2+} and Mg^{2+} concentrations are typically 33 and 11 ppm, respectively. As shown in Figure 3, the Pb removal rates were higher than 80%; in contrast, the removal rates for Ca^{2+} and Mg^{2+} were 5-15% and 3-10%, respectively. Therefore, the average Pb removal selectivity against Ca and Mg was as high as 292 and 158, respectively (Figure 3b), much higher than the numbers (1-7) using pristine AC in our previous report [16]. Note that increased removal rates were observed after running 7h, which is due to the decreased adsorption of Ca^{2+} and Mg^{2+}. For example, the removal rates at the first hour (C1) were approximately 15 and 5% for Ca and Mg and were approximately 5 and 3% at the 7th hour (7h-C1), respectively.

Surprisingly, however, no discharge of the adsorbed Pb^{2+} was observed during the discharge processes. As shown in Figure 3a, upon discharge the removal rates for Ca^{2+} and Mg^{2+} were negative, which means these cations did not discharge from the electrodes; in contrast, the Pb removal rates were still above 80%, instead of below zero, which indicates the Pb was removed rather than released. Meanwhile, extending the discharge time to 3 min did not make a difference (Figure 3a).

To determine the inability of the CDI cell to release Pb^{2+}, we first simulated the tap water while performing the regeneration with synthetic water containing 1 ppm Pb^{2+}, 30 ppm Ca^{2+}, and 10 ppm Mg^{2+}. We chose the Ca^{2+} and Mg^{2+} concentrations to be 30 and 10 ppm, respectively, to simulate the tap water in our office building. As shown in Figure 4, the four-layer-electrode CDI cell ran uninterrupted for 96 h by pumping the synthetic water. The CDI cell was charged for 8 min to remove ions, followed by a typical 2-min discharge to release the adsorbed ions. The initial Pb removal rate was approximately 85%, retained higher than 80% over 300 cycles and above 70% over 500 cycles. Low discharge rates of lead were observed (typically ~20%), but unlike the inability to discharge Pb in the case using tap water (Figure 3a). In contrast, the discharge rates for Ca^{2+} and Mg^{2+} were above 90%. The relatively low Pb discharge rate is related to the stronger bonding of thiol groups and Pb^{2+} ions, which resulted in an incomplete recovery for Pb^{2+} in 2 min. Pb discharge rates were observed by extending the discharge time to 3-5 min (Figure 4b); extending the discharge time to 8-10 min raised the Pb discharge rate above 100%, indicating the accumulated lead ion can be discharged. In other words, a deep discharge can help regenerate electrodes after a period of typical use cycles with a short discharge time; therefore, a long discharge time for each cycle is not necessary.

By comparing the regeneration performance with tap water and synthetic water, it was clear that the inability to discharge Pb^{2+} with tap water was related to a component in the tap water

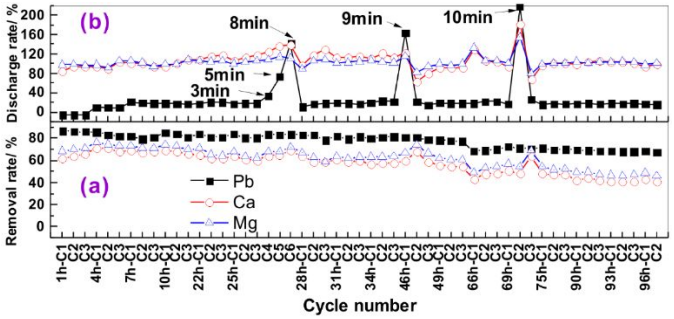

Figure 4. Regeneration performance of a four-layer-electrode cell with synthetic water, with 1 ppm Pb, 30 ppm Ca, and 10 ppm Mg at a flow rate of 23 mL min^{-1}: (a) Charge (10 min each cycle) and (b) discharge (2 min, or else if stated). Note that three groups of charge/discharge samples were taken at the first three cycles every 3 h, then the cell was kept running without sampling for 2.5 h.

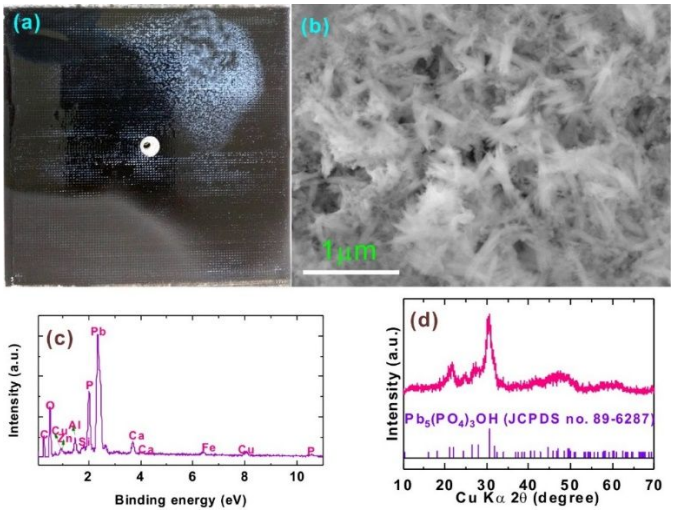

Figure 5. (a) Optical photo of an electrode after use, (b) SEM images, (c) EDS analysis, and (d) XRD pattern of the white precipitates collected from the electrode.

itself. To uncover the reason, the CDI cell was taken apart after running 24 h with the Pb-contaminated tap water; white precipitate was found in the mesh separator between the electrodes (Figure 5a). The white precipitate was examined by SEM, which showed needle-like morphology up to 1 μm in length (Figure 5b). The precipitate primarily consisted of Pb, P, and O, with minor components of Ca, Al, Fe, Cu, and Zn, as indicated by EDS analysis (Figure 5c). XRD characterization suggests the precipitate primarily consisted of $Pb_5(PO_4)_3(OH)$ (Figure 5d). Therefore, Pb was not released during discharge because the $Pb_5(PO_4)_3(OH)$ precipitate formed as a result of native phosphate ions in the tap water, which was absent in the synthetic water.

The mechanism for the formation of lead phosphates was investigated. Phosphate ions are popular in drinking water, which, according to WHO, helps to control pH value (approximately 8) and resist corrosion.[2] thereby suppressing the lead leaching from old lead-containing water pipes. Table S1 exhibits the typical orthophosphate ion concentrations, ranging between 0.08–1.87 ppm, in 10 top-population counties in Wisconsin in 2017; the values for Chicago and New York in 2017 were 1.12 and 2.10 ppm, respectively. The

solubility product contents of $Pb_3(PO_4)_2$ were as low as 8.0×10^{-43}, which easily leads to the formation of lead phosphate particulates in tap water, even when lead concentrations are very low. For example, with a Pb concentration of 1 ppm, phosphate ions are required at only 8.0×10^{-37} g L^{-1} to start forming particulates, which is much higher than the typical phosphate ion concentration in tap water (Table S1). A fresh tap water sample with 1 ppm lead was examined with a laser particle size analyser, presenting a mean particle size of 683 nm (Figure S5); such small particles in tap water stay suspended without forming precipitates. As an evidence, during the CDI test process no significant Pb concentration change was observed in the feeding tank containing 24 L tap water with 1 ppm Pb.

To help understand the effect of phosphate ions on CDI performance, an illustration scheme is presented in Figure S6. Without phosphates ions, cations and anions are adsorbed onto cathodes and anodes during charging and the concentrated ions are released as free ions upon discharging. In contrast, in the presence of phosphate ions, Pb contaminates are primarily suspended in tap water as particulates. The Pb particulates can be adsorbed onto the cathode during charging because they are negatively charged. Upon discharge the accumulated lead was released from the cathode, which formed precipitates with the concentrated phosphate ions from the anode. The resulting micro-sized precipitates can be removed with a filter.

Interestingly, with the assistance of the phosphate ions, no wastewater needs to be disposed. Upon charging the Pb is removed by electrochemically adsorbing onto electrode; during discharging the Pb is removed in the form of precipitates that can be filtrated, resulting in a new zero-wastewater CDI technique. In contrast, the water recovery with the conventional CDI technique is approximately 75%, because concentrated ions must be discharged as wastewater.

In summary, an MPS-GO/AC composite was prepared for selective lead ion removal against Ca^{2+} and Mg^{2+}. While very high Pb removal selectivity was observed during the single-pass CDI processes, no free Pb^{2+} was released in the case of tap water; instead, lead phosphate precipitates were collected due to the presence of phosphate ions. Because of the extremely low-solubility product content of lead phosphate, Pb exists in tap water in a form of particulate, which can be electrochemically attracted to cathodes upon charging. The accumulated Pb particulates are released and form precipitates with the concentrated phosphates ions from anodes, which can be removed with an additional filter, resulting in no wastewater. A comparison of relevant CDI removal of Pb^{2+} is shown in Table S2 to highlight the advance in this study.

Besides lead, other heavy-metal ions (such as Cu, Cd, and Ni) also can be selectively removed against Ca and Mg ions, because their solubility product contents of $Cu_3(PO_4)_2$ (1.40×10^{-37}), $Cd_3(PO_4)_2$ (2.53×10^{-33}), and $Ni_3(PO_4)_2$ (4.74×10^{-32}) are at least two orders of magnitude smaller than those of $Ca_3(PO_4)_2$ (2.07×10^{-29}) and $Mg_3(PO_4)_2$ (1.04×10^{-24}). Therefore, with the help of native phosphate ions in tap water, multiple heavy metals (e.g., lead, copper, cadmium, nickel) can be selectively removed against calcium and magnesium ions in such a zero-wastewater CDI. This shows promising applications in water treatment, especially in drinking water systems.

Acknowledgments

This project was supported by the National Science Foundation Industry/University Cooperative Research Center on Water Equipment & Policy located at University of Wisconsin-Milwaukee (IIP-1540032) and Marquette University (IIP-1540010). J. H. Chen acknowledges support by (while serving at) the U.S. National Science Foundation. The authors acknowledge Mike Beck (Pentair), Seong-Hoon Yoon (Nalco Water), Kyle Wood (Nalco Water), Kuldip Kumar (MWRD Chicago), Craig Schmitt (Watts Water), Steven D. Jons (Dow Chemical Company), Luke Franklin (Dow Chemical Company), Mark Gehring (Dow Chemical Company), and Bruce Taylor (KX Technologies) for their useful advices and discussions. The authors also thank Eric Ritzel (University of Wisconsin-Milwaukee) for providing useful information about the water quality data.

Conflicts of interest

There are no conflicts to declare.

Notes and references

1 US EPA: National Primary Drinking Water Regulations, 2016, 7.
2 World Health Organization: Nutrients in drinking water, 2005.
3 World Health Organization: Lead in Drinking-water, 2011, 1-26.
4 Milwaukee Water Works: 2017 Distribution System Water Quality, 2018.
5 E. Buyuktuncel, A. Tuncel, O. Genc and A. Denizli, Selective removal of lead ions by polyethylene glycol methacrylate gel beads carrying Cibacron Blue F3GA, *Sep. Sci. Technol.* , 2001, 36, 3427-3438.
6 Y. H. Deng, Z. Q. Gao, B. Z. Liu, X. B. Hu, Z. B. Wei and C. Sun, Selective removal of lead from aqueous solutions by ethylenediamine-modified attapulgite, *Chem. Eng. J.* , 2013, 223, 91-98.
7 H. T. Fan, X. T. Sun and W. X. Li, Sol-gel derived ion-imprinted silica-supported organic-inorganic hybrid sorbent for selective removal of lead(II) from aqueous solution, *J. Sol-Gel Sci. Technol.* , 2014, 72, 144-155.
8 H. T. Fan, X. T. Sun, Z. G. Zhang and W. X. Li, Selective Removal of Lead(II) from Aqueous Solution by an Ion-Imprinted Silica Sorbent Functionalized with Chelating N-Donor Atoms, *J. Chem. Eng. Data* 2014, 59, 2106-2114.
9 S. Y. Kazemi, A. S. Hamidi and M. J. Chaichi, Kinetics study of selective removal of lead(II) in an aqueous solution containing lead(II), copper(II) and cadmium(II) across bulk liquid membrane, *J. Iran. Chem. Soc.* , 2013, 10, 283-288.
10 R. Khani, S. Sobhani and M. H. Beyki, Highly selective and efficient removal of lead with magnetic nano-adsorbent: Multivariate optimization, isotherm and thermodynamic studies, *J. Colloid Interface Sci.* , 2016, 466, 198-205.

11 A. Sdiri, M. Khairy, S. Bouaziz and S. El-Safty, A natural clayey adsorbent for selective removal of lead from aqueous solutions, *Appl. Clay Sci.* , 2016, 126, 89-97.
12 Q. Su, B. C. Pan, S. L. Wan, W. M. Zhang and L. Lv, Use of hydrous manganese dioxide as a potential sorbent for selective removal of lead, cadmium, and zinc ions from water, *J. Colloid Interface Sci.* , 2010, 349, 607-612.
13 Y. Y. Wu, X. L. Cheng, X. F. Zhang, Y. M. Xu, S. Gao, H. Zhao and L. H. Huo, High efficient and selective removal of Pb^{2+} through formation of lead molybdate on alpha-MoO_3 porous nanosheets array, *J. Colloid Interface Sci.* , 2017, 491, 80-88.
14 Z. L. Zhang, X. D. Zhang, D. C. Niu, Y. S. Li and J. L. Shi, Highly efficient and selective removal of trace lead from aqueous solutions by hollow mesoporous silica loaded with molecularly imprinted polymers, *J. Hazard. Mater.* , 2017, 328, 160-169.
15 M. M. Chen, D. Wei, W. Chu, T. Wang and D. G. Tong, One-pot synthesis of O-doped BN nanosheets as a capacitive deionization electrode for efficient removal of heavy metal ions from water, *J. Mater. Chem. A*, 2017, 5, 17029-17039.
16 Q. Dong, X. Guo, X. Huang, L. Liu, R. Tallon, B. Taylor and J. Chen, Selective removal of lead ions through capacitive deionization: Role of ion-exchange membrane, *Chem. Eng. J.* , 2019, 361, 1535-1542.
17 L. J. Liu, X. R. Guo, R. Tallon, X. K. Huang and J. H. Chen, Highly porous N-doped graphene nanosheets for rapid removal of heavy metals from water by capacitive deionization, *Chem. Commun.* , 2017, 53, 881-884.
18 Q. H. Ji, C. Z. Hu, H. J. Liu and J. H. Qu, Development of nitrogen-doped carbon for selective metal ion capture, *Chem. Eng. J.* , 2018, 350, 608-615.
19 P. Y. Liu, T. T. Yan, J. P. Zhang, L. Y. Shi and D. S. Zhang, Separation and recovery of heavy metal ions and salt ions from wastewater by 3D graphene-based asymmetric electrodes via capacitive deionization, *J. Mater. Chem. A*, 2017, 5, 14748-14757.
20 J. L. Han, L. Y. Shi, T. T. Yan, J. P. Zhang and D. S. Zhang, Removal of ions from saline water using N, P co-doped 3D hierarchical carbon architectures via capacitive deionization, *Env. Sci. -Nano*, 2018, 5, 2337-2345.
21 Z. U. Khan, T. T. Yan, L. Y. Shi and D. S. Zhang, Improved capacitive deionization by using 3D intercalated graphene sheet-sphere nanocomposite architectures, *Env. Sci. -Nano*, 2018, 5, 980-991.
22 T. T. Yan, J. Liu, H. Lei, L. Y. Shi, Z. X. An, H. S. Park and D. S. Zhang, Capacitive deionization of saline water using sandwich-like nitrogen-doped graphene composites via a self-assembling strategy, *Env. Sci. -Nano*, 2018, 5, 2722-2730.
23 K. C. Zuo, J. Kim, A. Jain, T. X. Wang, R. Verduzco, M. C. Long and Q. L. Li, Novel Composite Electrodes for Selective Removal of Sulfate by the Capacitive Deionization Process, *Environ. Sci. Technol.* , 2018, 52, 9486-9494.
24 C. Y. Lee, Q. Van Le, C. Kim and S. Y. Kim, Use of silane-functionalized graphene oxide in organic photovoltaic cells and organic light-emitting diodes, *PCCP* 2015, 17, 9369-9374.
25 W. Li, B. Q. Zhou, M. Y. Wang, Z. H. Li and R. Ren, Silane functionalization of graphene oxide and its use as a reinforcement in bismaleimide composites, *J Mater Sci*, 2015, 50, 5402-5410.
26 S. P. Lonkar, Y. S. Deshmukh and A. A. Abdala, Recent advances in chemical modifications of graphene, *Nano Res*, 2015, 8, 1039-1074.
27 S. S. Abbas, G. J. Rees, N. L. Kelly, C. E. J. Dancer, J. V. Hanna and T. McNally, Facile silane functionalization of graphene oxide, *Nanoscale*, 2018, 10, 16231-16242.
28 J. Y. Zhang, T. D. Ding, Z. J. Zhang, L. P. Xu and C. L. Zhang, Enhanced Adsorption of Trivalent Arsenic from Water by Functionalized Diatom Silica Shells, *Plos One*, 2015, 10.
29 S. R. Zahabi, S. A. H. Ravandi and A. Allafchian, Removal of nickel and cadmium heavy metals using nanofiber membranes functionalized with (3-mercaptopropyl)trimethoxysilane (TMPTMS), *J. Water health* 2016, 14, 630-639.
30 Z. Y. Xia, L. Baird, N. Zimmerman and M. Yeager, Heavy metal ion removal by thiol functionalized aluminum oxide hydroxide nanowhiskers, *Appl. Surf. Sci.* , 2017, 416, 565-573.
31 B. Viltuznik, A. Kosak, Y. L. Zub and A. Lobnik, Removal of Pb(II) ions from aqueous systems using thiol-functionalized cobalt-ferrite magnetic nanoparticles, *J. Sol-Gel Sci. Technol.* , 2013, 68, 365-373.
32 L. N. H. Arakaki, M. G. da Fonseca, E. C. da Silva, A. P. D. Alves, K. S. de Sousa and A. L. P. Silva, Extraction of Pb(II), Cd(II), and Hg(II) from aqueous solution by nitrogen and thiol functionality grafted to silica gel measured by calorimetry, *Thermochim. Acta* 2006, 450, 12-15.
33 Z. Z. Xie, X. H. Shang, J. B. Yan, T. Hussain, P. F. Nie and J. Y. Liu, Biomass-derived porous carbon anode for high-performance capacitive deionization, *Electrochim. Acta* 2018, 290, 666-675.
34 P. A. Chen, H. C. Cheng and H. P. Wang, Activated carbon recycled from bitter-tea and palm shell wastes for capacitive desalination of salt water, *Journal of Cleaner Production*, 2018, 174, 927-932.
35 R. H. Tian, O. Seitz, M. Li, W. C. Hu, Y. J. Chabal and J. M. Gao, Infrared Characterization of Interfacial Si-O Bond Formation on Silanized Flat SiO_2/Si Surfaces, *Langmuir*, 2010, 26, 4563-4566.
36 W.-H. Chen, Y.-T. Tseng, S. Hsieh, W.-C. Liu, C.-W. Hsieh, C.-W. Wu, C.-H. Huang, H.-Y. Lin, C.-W. Chen, P.-Y. Lin and L.-K. Chau, Silanization of solid surfaces via mercaptopropylsilatrane: a new approach of constructing gold colloid monolayers, *RSC Adv.* , 2014, 4, 46527-46535.
37 A. G. El-Deen, R. M. Boom, H. Y. Kim, H. Duan, M. B. Chan-Park and J. H. Choi, Flexible 3D Nanoporous Graphene for Desalination and Bio-decontamination of Brackish Water via Asymmetric Capacitive Deionization, *ACS Appl. Mater. Interfaces*, 2016, 8, 25313-25325.
38 K. Laxman, M. T. Z. Myint, R. Khan, T. Pervez and J. Dutta, Improved desalination by zinc oxide nanorod induced electric field enhancement in capacitive deionization of brackish water, *Desalination*, 2015, 359, 64-70.
39 K. Laxman, M. T. Z. Myint, R. Khan, T. Pervez and J. Dutta, Effect of a semiconductor dielectric coating on the salt adsorption capacity of a porous electrode in a capacitive deionization cell, *Electrochim. Acta* 2015, 166, 329-337.
40 D. Jiao, C. King, A. Grossfield, T. A. Darden and P. Y. Ren, Simulation of Ca^{2+} and Mg^{2+} solvation using polarizable atomic multipole potential, *J. Phys. Chem. B* 2006, 110, 18553-18559.
41 D. Di Tommaso and N. H. de Leeuw, Structure and dynamics of the hydrated magnesium ion and of the solvated magnesium carbonates: insights from first principles simulations, *PCCP* 2010, 12, 894-901.
42 Milwaukee Water Works: 2018 Distribution System Water Quality, 2019.

COMMUNICATION

TOC